Mathematical and Computational Applications

MDPI

Article

Vibration Control of Light Bridges Under Moving Loads Using Nonlinear Semi-Active Absorbers

Hamed Saber [1], Farhad S. Samani [1], Francesco Pellicano [2], Moslem Molaie [2] and Antonio Zippo [2,*]

[1] Department of Mechanical Engineering, Shahid Bahonar University of Kerman, Kerman 76169-14111, Iran; hamed3071@yahoo.com (H.S.)
[2] Department of Engineering "Enzo Ferrari", University of Modena and Reggio Emilia, 41121 Modena, Italy; francesco.pellicano@unimore.it (F.P.); moslem_molaie@unimore.it (M.M.)
* Correspondence: antonio.zippo@unimore.it

Abstract: The dynamic response of light bridges to moving loads presents significant challenges in controlling vibrations that can impact on the structural integrity and the user comfort. This study investigates the effectiveness of nonlinear semi-active absorbers in mitigating these vibrations on light bridges that are particularly susceptible to human-induced vibrations, due to their inherent low damping and flexibility, especially under near-resonance conditions. Traditional passive vibration control methods, such as dynamic vibration absorbers (DVAs), may not be entirely adequate for mitigating vibrations, as they require adjustments in damping and stiffness when operating conditions change over time. Therefore, suitable strategies are needed to dynamically adapt DVA parameters and ensure optimal performance. This paper explores the effectiveness of linear and nonlinear DVAs in reducing vertical vibrations of lightweight beams subjected to moving loads. Using the Bubnov-Galerkin method, the governing partial differential equations are reduced to a set of ordinary differential equations and a novel nonlinear DVA with a variable damping dashpot is investigated, showing better performances compared to traditional constant-parameter DVAs. The nonlinear viscous damping device enables real-time adjustments, making the DVA semi-active and more effective. A footbridge case study demonstrates significant vibration reductions using optimized nonlinear DVAs for lightweight bridges, showing broader frequency effectiveness than linear ones. The quadratic nonlinear DVA is the most efficient, achieving a 92% deflection reduction in the 1.5–2.5 Hz range, and under running and jumping reduces deflection by 42%.

Keywords: bridge vibrations; semi-active DVA; adjustable vibration absorber; viscous variable damping dashpot; moving load; vibration reduction

Academic Editor: Nicholas Fantuzzi

Received: 23 December 2024
Revised: 10 February 2025
Accepted: 10 February 2025
Published: 14 February 2025

Citation: Saber, H.; Samani, F.S.; Pellicano, F.; Molaie, M.; Zippo, A. Vibration Control of Light Bridges Under Moving Loads Using Nonlinear Semi-Active Absorbers. *Math. Comput. Appl.* **2025**, *30*, 19. https://doi.org/10.3390/mca30010019

1. Introduction

Reducing vibrations is important for the serviceability and safety of light structures like bridges. The bridge structure may experience significant deflections when subjected to a moving load in near resonance conditions. There are multiple methods to reduce beam vibrations, including selecting the appropriate structural material, control of the bridge's overall condition and support strengthening, and utilizing the dynamic vibration absorber (DVA) as the most efficient technique. Samani and Pellicano [1] studied the efficacy of linear and nonlinear dampers installed on simply-supported beams subjected to moving loads. The performance of the suggested vibration absorber was evaluated based on the maximum vibration amplitude and the energy dissipation by the damper. Additionally, Samani et al. [2] conducted a study comparing the effectiveness of linear and

nonlinear DVAs under dynamic loads from moving vehicles. Their findings indicated that cubic stiffness is more effective than linear stiffness. They suggested that enhancing the nonlinearity of stiffness leads to a more efficient reduction in beam deflection.

Recently, many researchers investigated the impact of the vertical component of moving loads on lightweight bridges and evaluating the efficiency of linear DVAs in mitigating induced vibrations [3–8]. Saber et al. examined how different types of DVAs can reduce vibrations in footbridges. The DVAs were fine-tuned through two methods: minimizing beam deflection and maximizing the absorbed energy by the vibration absorber [9]. Caprani and Ahmadi [10] investigated human-structure interaction models for vertical vibration induced by pedestrian excitation; in their study, the beam equation is analyzed using modal coordinates and the finite element method in the referenced study. Kei Ao and Reynolds [11] investigated an Eddy Current Damper as an alternative to the traditional viscous dampers in civil engineering structures; the damper was based on electromagnetic induction and minimal friction, it showed promising damping properties when applied to a footbridge. Finite element and analytical models confirmed its effectiveness in enhancing damping under various loading conditions. In another study, the same authors investigated the design and effectiveness of an electromagnetic shunt damper using an electrodynamic actuator to improve vibration control in civil engineering structures, specifically footbridges, by comparing its performance to a tuned mass damper. H_∞ and H_2 optimization techniques were applied to enhanced the dissipation across multiple vibration modes [12]. Pedersen and Frier [13] researched how footbridge vibrations are influenced by walking parameters by analyzing the response of a footbridge to pedestrian load models. Lievens et al. [14] demonstrated that forecasting the dominant characteristics of the finite element (FE) models of the bridges is challenging. Furthermore, the modal parameters will change over time due to variations in environmental conditions. Nimmen et al. [15] proposed that significant changes in the natural frequencies between the finite element analysis outcomes and the experimental data may arise from the assumptions incorporated in the FE model, including boundary conditions, material properties, and the impact of non-structural components.

Ding and Chen [16] carried out an extensive analysis of studies regarding nonlinear vibration absorbers. Their work focuses on the design, analysis, conclusions, and uses of nonlinear vibration absorber tools to enhance vibration mitigation in engineering contexts. Gourdon et al. [17] investigated the robustness of a new cubic nonlinear energy sink; they experimentally validated the theoretical findings through tests on a reduced-scale building model. Their findings suggest that nonlinear attachments can outperform linear ones. Ferreira et al. [18] studied semi-active dampers to mitigate synchronous lateral vibrations in pedestrian bridges. Their numerical analysis showed that the new semi-active vibration absorber could achieve similar performance of a passive absorber but requires a small mass. The DVA's self-tuning capability makes it more effective in addressing multimode control compared to a traditional passive linear Tuned Mass Damper (TMD). Maslanka [19] introduced a semi-active vibration absorber that incorporates acceleration and relative motion feedbacks optimized using frequency domain analysis. This particular variation of semi-active DVA includes a controllable viscous damper with magnetorheological properties. Saber et al. [20], presented an innovative nonlinear viscous dashpot with tunable damping for DVAs. In another study, Saber et al. [6] investigated how vibration absorbers can reduce vertical deflections of footbridges caused by various types of human activities. Chen et al. [21], investigated the influence of human-induced load models on the effectiveness of a tuned mass damper in dampening vibrations in a floor. They analyzed the floor's reactions to different types of excitations and showed that employing distinct load models, like those for walking or jumping, can greatly alter the performance of the TMD. Recently,

Nguyen et al. [22] investigated the use of semi-active tuned mass dampers (STMD) to mitigate resonant vibrations in railway bridges subjected to high-speed trains. Unlike passive controllers, which have a narrow operational bandwidth and are vulnerable to detuning, the STMD enhances the vibration suppression across a broader frequency range, demonstrating improved robustness and effectiveness in real-world conditions. Kumar and Bhushan [23], developed an innovative semi-active absorber that utilizes Magnetorheological fluids and elastomers to achieve variable damping and stiffness. Their mathematical model demonstrated significant improvements versus the passive technologies. Barrera-Vargas et al. [24], investigated semiactive tuned mass dampers for lightweight pedestrian structures. The study presented a design methodology that reduces structural acceleration and inertial forces. Simulations showed that STMDs effectively mitigate vibrations while reducing inertial mass compared to passive systems. Wang et al. [25], introduced a novel magnetorheological damper featuring an elastic ring to enhance the damper performance by optimizing the oil-film thickness distribution. Such device can be categorized as semi-active; through dynamic modeling and experimental validation, the study highlighted the improved damping characteristics compared to conventional systems. For more information on the effectiveness of nonlinearity on vibration mitigation of various test cases, the reader is suggested to analyze Refs. [26–30].

The major contribution of the present paper is the introduction of a nonlinear DVA having a viscous variable damping dashpot; more specifically, this study introduces a quadratic nonlinearity to the damping element, allowing variable damping constants based on flow rates. This newly proposed dashpot enhances the performance of the dynamic system, i.e., a footbridge subjected to moving pedestrians. The classical linear DVA typically reduces vibrations within a narrow frequency band, whereas a nonlinear DVA can operate effectively across a wider spectrum. This study investigates various types of nonlinear DVAs applied to footbridges, comparing their performance with the standard linear DVAs (Tigli and Den Hartog formulation), thereby illustrating the advantages of nonlinearity. The test case for the application of linear and nonlinear DVAs is an Euler-Bernoulli beam, simulating a pedestrian bridge, the partial differential equations (PDEs) are reduced to ordinary differential equations (ODEs) by means of the Bubnov-Galerkin and numerically integrated using the Gauss-Kronrod method. This innovative design allows for real-time adjustments of damping parameters, which is crucial for effectively mitigating vibrations caused by moving loads on light bridges. This adaptability represents a substantial improvement over traditional passive systems that operate with fixed parameters, thereby enhancing performance under varying load conditions.

Furthermore, this paper considers a nonlinear semi-active absorber as a semi-active device capable of adapting its properties in real-time using adjustable elements. Specifically, two types of nonlinearities are proposed: geometric cubic nonlinearity and quadratic nonlinear damping. However, this work does not focus on control algorithms or the engineering implementation of the application.

2. Moving Load Bridge Interaction Model

The governing equations of the beam with DVA, subjected to a moving load, are derived by projecting the PDE of the domain, obtaining the mass, damping, and stiffness matrices of the system. This involves considering the contributions from both the beam and the absorber, where the inertia effect of the spring mass is accounted for to ensure accurate modeling of the dynamic responses. The effective overall matrices are obtained by applying the appropriate boundary conditions, leading to a comprehensive representation of the beam's dynamics under the moving load [31].

A DVA is connected to the bridge to dampen the vibrations, as shown in Figure 1. As mentioned above, the PDE, which governs the bridge's dynamics, including the associated boundary and initial conditions, is the follow:

$$EIw_{,xxxx}(x,t) + \rho A w_{,tt}(x,t) + [f(u) + g(u_{,t})]\delta(x-d) = F(x,t) \quad x \in (0,L), \quad t > 0 \tag{1}$$

$$w(0,t) = 0, \quad w(L,t) = 0, \quad w_{,xx}(0,t) = 0, \quad w_{,xx}(L,t) = 0 \tag{2}$$

$$w(x,0) = 0, \quad w_{,t}(x,0) = 0, \quad u(t) = w(d,t) - z(t) \tag{3}$$

$$w_{,t} = \frac{\partial w}{\partial t}, \; w_{,tt} = \frac{\partial^2 w}{\partial t^2}, \; w_{,xxxx} = \frac{\partial^4 w}{\partial x^4} \tag{4}$$

The moment of inertia of the beam's cross-sectional area is denoted by I, while ρ represents the material density, and A represents the beam's cross-section area. The functions $g(u_{,t})$, and $f(u)$ represent the restoring forces of the dashpot, and spring of the DVA, respectively. The term $[f(u) + g(u_{,t})]\delta(x-d)$ denotes the force applied by the DVA to the bridge; The damper location on the bridge is in the midspan $d = L/2$. The vertical position of the DVA's mass (m_0) is denoted by $z(t)$, while the vertical displacement of the bridge is denoted by $w(x,t)$. The relative displacement of the DVA's mass and the beam mid-span is denoted by $u(t)$, as shown in Equation (3).

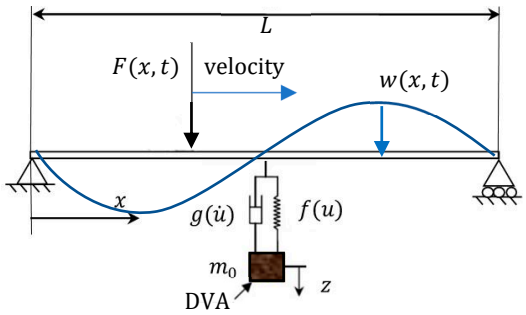

Figure 1. A bridge structure featuring a vibration absorber connected to it, exposed to a dynamic force.

The equation for the moving force can be expressed as follows:

$$F(x,t) = G(t)\,\delta(x - vt)\left[H\left(\frac{L}{v} - t\right)\right] \tag{5}$$

The Dirac delta, and Heaviside functions are denoted by δ and $H(t)$, respectively. The amplitude of the total force exerted by the moving force is denoted as $G(t)$. The governing equations of the DVA reads:

$$m_0 z_{,tt} - ku - \lambda u_{,t}(t) = 0, \qquad t > 0 \tag{6}$$

$$z(0) = 0, \qquad z_{,t}(0) = 0, \qquad t > 0 \tag{7}$$

The position of the mass (m_0) of the DVA, $z(t)$, is represented in Equation (7).

The displacement field of the beam is expanded using the eigenfunctions of a free homogeneous beam, see Equation (8):

$$w(x,t) = \sum_{r=1}^{N} q_r(t)\varphi_r(x) \tag{8}$$

The modal coordinates are denoted by $q_r(t)$, the normalized eigenfunctions are represented by $\varphi_r(x)$, and the number of modes in the system is indicated by N. The definition of the eigenfunctions is as follows:

$$\varphi_r(x) = \left(\frac{2}{mL}\right)^{\frac{1}{2}} \sin\left(\frac{r\pi x}{L}\right), \quad \omega_r = (r\pi)^2 \left(\frac{EI}{mL^4}\right)^{\frac{1}{2}}, \quad r = 1, 2, 3, \ldots \tag{9}$$

The beam's mass per unit length is represented as $m = \rho A$, and the natural circular frequency of the rth mode is denoted as ω_r. Notably the eigenfunctions must satisfy the boundary conditions of the problem. The Bubnov-Galerkin method is used to project the PDE into the eigenfunction basis and the resulting ODEs are numerically integrated with the Gauss-Kronrod method, which employs adaptive Gaussian quadrature with error estimation evaluated at Kronrod points.

The optimization strategy used for determining the optimal parameters is a brute force approach, that involves exploring the full parameter space, the method that is computationally intensive but effective (see Refs. [2,32–35]).

The jth modal equation can be expressed as follows:

$$\ddot{q}_r + 2\xi_r \omega_r \dot{q}_r + \omega_r^2 q_r + \{f(u) + g(u_{,t})\}\varphi_r(d) = \varphi_r(vt)G(t) \tag{10}$$

$f(u)$, and $g(u_{,t})$ are expressed as the equations below:

$$f(u(t)) = k\left[\sum_{r=1}^{N} q_r(t)\varphi_r(d) - z(t)\right]^{\alpha} \left|\sum_{r=1}^{N} q_r(t)\varphi_r(d) - z(t)\right|^{\beta} \tag{11}$$

$$g(u_{,t}(t)) = \lambda\left[\sum_{r=1}^{N} \dot{q}_r(t)\varphi_r(d) - \dot{z}(t)\right]^{\gamma} \left|\sum_{r=1}^{N} \dot{q}_r(t)\varphi_r(d) - \dot{z}(t)\right|^{\delta} \tag{12}$$

The DVA's stiffness is denoted by k, while its damping is represented by λ. These values will be calculated using both numerical and analytical methods in the upcoming sections. The symbol ξ_r represents the damping ratio of the bridge.

3. Improving the DVA Parameters to Enhance Performance

This paper examines two objective functions for the optimization procedure. The primary aim of the optimization is to reduce the highest beam deflection, and the secondary goal is to increase the energy dissipated by the DVA (η), which is computed using Equation (13), as follows:

$$\eta = E_{DVA}/E_{in} = \frac{\int_0^{t_1} \lambda\left[\dot{z}(t) - \sum_{r=1}^{N} \dot{q}_r(t)\varphi_r(d)\right]^m \left|\dot{z}(t) - \sum_{r=1}^{N} \dot{q}_r(t)\varphi_r(d)\right|^n dt}{\int_0^{t_0} F_i\left[\dot{q}_r(t)\varphi_r(x_F)\right] dt} \tag{13}$$

The energy dissipated by the viscous damper of the DVA (E_{DVA}) is referred to as a nonlinear energy sink, see Refs. [1,27,36]. F_i symbolizes the force applied by the pedestrian, as defined in Equation (9). The pedestrian's position on the footbridge is denoted by x_F, which is equal to vt. The energy absorbed by the DVA is denoted as E_{DVA}, and E_{in} is the energy input from the pedestrian's feet on the bridge. The values of the integer powers m and n depend on whether a linear or nonlinear damper is utilized in diverse DVAs. The time t_1 is chosen to be long enough to ensure damping of the transient response, while t_0 corresponds to the period for which the load acts on the beam. The objective of this approach is to enhance the dissipation of energy by the DVA [1].

Figure 2 presents a flowchart outlining the steps of the computer algorithm used to solve the equations of the human-structure interaction system.

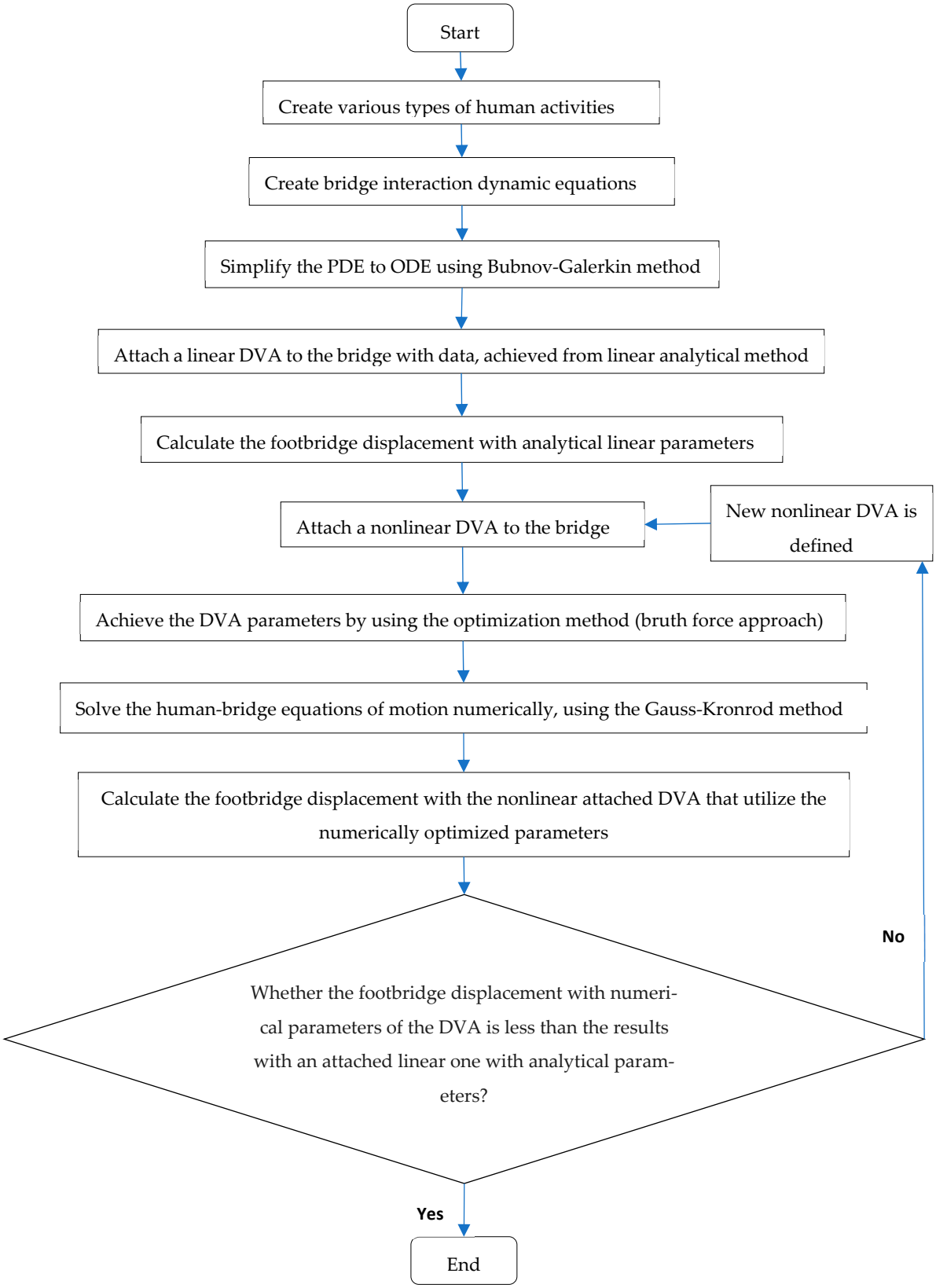

Figure 2. Flowchart outlining the steps of the computer algorithm used to solve the equations of the human-structure interaction system with attached DVA.

4. Effect of Force Amplitude and Velocity on the Optimal Values of the DVA

This section explores how force parameters like amplitude and velocity affect the optimized characteristics of the DVA, including damping and stiffness. Chen et al. studied how the load models affect the performance of a tuned mass damper in reducing vibrations in a floor [21]. They compared the floor's responses to various types of excitations and demonstrated that different load models, significantly impact the effectiveness of the tuned mass damper. Sayyad and Gadhave [37] researched a variable stiffness magnetic vibration absorber to reduce vibration in a beam structure when exposed to varying frequency harmonic excitation, aiming to decrease vibration in the main system. The present study investigates the effectiveness of various linear and nonlinear DVAs in reducing vibrations on a lightweight bridge. It considers pedestrian movement as a moving load on the bridge and explores how variations in force amplitude and velocity affect the reduction of vibrations.

4.1. Performance Analysis of Different Types of Vibration Absorbers Under Pedestrian Excitation

The vertical force generated by the pedestrian's feet is typically similar in magnitude and can be estimated by using a sine function, as illustrated in Equation (14); see [38,39].

$$G(t) = W + \sum_{k=1}^{h} W\eta_k \sin\left(2\pi k f_p\, t + \varphi_k\right) \tag{14}$$

In Equation (14), the weight of the pedestrian is represented by W, calculated as $W = m_p g$. The variable f_p represents the pedestrian's pacing rate, which is determined by the pedestrian's velocity (v) and stride length (l_p), expressed as $f_p = v/l_p$ [11]. As mentioned in Ref. [40], the coefficient in the Fourier series denoted by η_k is known as the "dynamic load factor (DLF)", while the harmonic phase angle, represented by φ_k, can be selected randomly and uniformly within the range of $[-\pi, \pi]$. Ref. [41] suggested DLF values for the first four harmonics, computed based on an assumed walking frequency between 1 and 2.8 Hz, as described in Equation (15).

$$\begin{array}{ll} \eta_{1W} = 0.37\left(f_p - 0.95\right) \le 0.5 & 1 \le f_p \le 2.8 \text{ Hz} \\ \eta_{2W} = 0.054 + 0.0044 f_p & 2 \le f_p \le 5.6 \text{ Hz} \\ \eta_{3W} = 0.026 + 0.0050 f_p & 3 \le f_p \le 8.4 \text{ Hz} \\ \eta_{4W} = 0.010 + 0.0051 f_p & 4 \le f_p \le 11.2 \text{ Hz} \end{array} \tag{15}$$

To evaluate the accuracy of the aforementioned models, the force exerted on the footbridge by a walking pedestrian over time is analyzed and compared with the results from Kim et al. [42], which originally based their findings on the experimental investigation conducted by Wu et al. [43]. In the present study, the first four dynamic load factors for running and jumping pedestrians are derived from Rainer et al. [44]. Notably, the typical frequency of walking excitation ranges from 1.6 to 2.4 Hz [45], while the frequencies for running and jumping are between 2 and 3 Hz [44]. The system of Equation (15) is considered at a frequency of 2 Hz, and the first four DLFs are specified in Table 1. The footbridge characteristics is described in Table 2. The pedestrian weighs 724 Newtons.

Table 1. DLFs are used for regular walking at a rate of 2 Hz [9].

Reference	η_{1W}	η_{2W}	η_{3W}	η_{4W}
[25]	0.40	0.10	0.10	0

Table 2. Footbridge characteristics.

Unit Mass	Length	Cross-Section Area	Area Moment of Inertia	Fundamental Frequency	Damping Ratio	Modulus of Elasticity
500 $\frac{\text{kg}}{\text{m}}$	50 m	1.07 m^2	0.0255 m^4	2 Hz	0.004	200 GPa

In this study, the initial four phase angles of a walking pedestrian involved in any task are $\varphi_1 = 0$, $\varphi_2 = -\pi/2$, $\varphi_3 = -\pi/2$, $\varphi_4 = 0$ radians, as stated in [25]. The study's formulation accuracy for a walking pedestrian is assessed in Figure 3 using the research findings of [25].

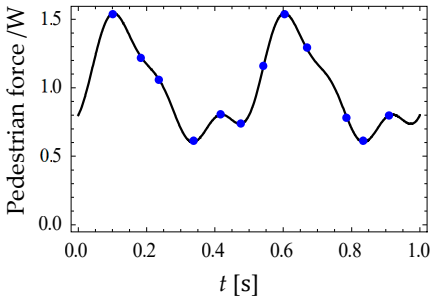

Figure 3. The force-time response produced by a walking person with a frequency of 2 Hz; —-: the model presented in Equation (14); filled circles •: extracted data from [25].

Different nonlinear DVAs incorporating quadratic and cubic nonlinearity are utilized on the footbridges in the subsequent sections.

To verify the effectiveness of nonlinear DVAs under moving loads, we used data from Samani and Pellicano [1]; their study involved a nonlinear DVA with cubic stiffness and linear damping attached to a bridge; they presented the maximum mid-span deflection of the beam versus the stiffness of the nonlinear absorber. Notably, to check the accuracy of our formula in this paper we considered a constant amplitude moving force as stated in Ref. [1]. In Figure 4, one-mode and five-mode expansions are shown as dashed and solid green lines, respectively, with the five-mode expansion aligning well with the data marked by red points in Ref. [1]. The results demonstrate a strong agreement between the five-mode expansion model used in this study and the data obtained from Ref. [1].

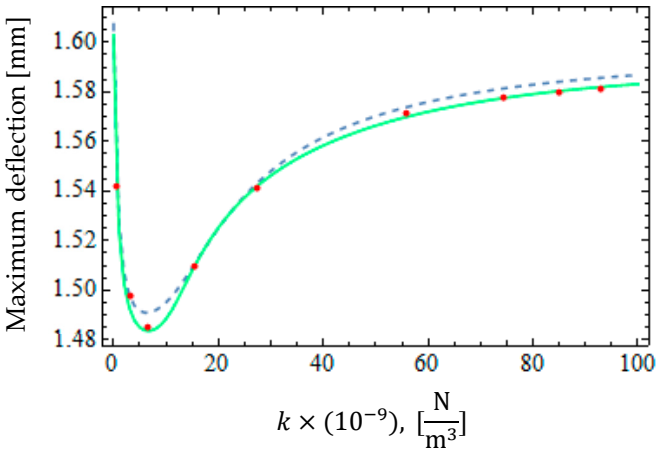

Figure 4. Verification of the bridges subjected to moving load with constant amplitude an attached DVA (cubic stiffness and linear damping) with the data extracted from Ref. [1].

4.1.1. The Optimal Configuration for a Linear DVA

To minimize the resonance effects of a beam subjected to a periodic load, it is essential to calculate the beam's equivalent mass, which is affected by the positioning of the vibration absorber. According to Den Hartog's method, the ideal stiffness and damping settings for the linear DVA attached to a simply supported beam are recommended as follows:

$$k = m_0 \left(\frac{\omega_1}{1+\mu} \right)^2 \tag{16}$$

$$\lambda = 2m_0\omega_1 \sqrt{\frac{3\mu}{8(1+\mu)^3}} \tag{17}$$

where ω_1 represents the primary natural frequency of the beam, μ is the ratio of m_0/m_e, where $m_e = mL/2\,(sin\,\frac{\pi d}{L})^2$ represents the equivalent mass of the beam. Den Hartog's method determines the optimal values of λ and k as 5293 Ns/m and 164 kN/m, respectively, as per Equations (16) and (17). The optimal solutions for both objective functions will be achieved using the numerical approach detailed in Section 2. The main focus will be on the region where the highest efficiency (η) and lowest deflection is observed. The ranges for the parameters λ and k are from 0 to 10 kNs/m and from 50 kN/m to 300, respectively. By systematically varying the viscous damping and stiffness across a 50×50 grid with damping and stiffness increments of 0.2 kNs/m and 5 kN/m, respectively, the minimum deflection can be ascertained. The optimized values of λ and k for the energy-related objective function represent the points at which the DVA dissipates the maximum energy. Figure 5A,B illustrate the energy and deflection optimization approaches, respectively. The optimal parameters for λ and k, using a linear DVA for each approach, are also presented. In Figure 6A, Peaks A, B, and C depict the minimum values of the optimized DVA when utilizing the energy method. These peaks signify the least favorable situations for the optimized DVA across the anticipated frequency range of excitation. By substituting $m = 2$ and $n = 0$ into Equation (13), an efficiency of 92.80% (at point C) is attained, as illustrated in Figure 6A, for $\lambda = 6.4$ kNs/m and $k = 145$ kN/m, obtained from Figure 5A. The optimum λ and k values for the deflection method are determined by finding the combination that minimizes the maximum deflection for each frequency. The optimal parameters of $\lambda = 6$ kNs/m and $k = 180$ kN/m lead to a minimum deflection of 0.96 mm, identified through a thorough search utilizing the deflection function shown in Figure 5B. It is important to highlight that the integer powers for a linear DVA in Equations (11) and (12) are: $\alpha = 1$, $\beta = 0$, $\gamma = 1$ and $\delta = 0$. It should be noted that, in a linear DVA, the integer powers differ between the two optimization methods. The crucial difference lies in the fact that in the energy optimization approach, the footbridge's time response would exhibit quicker damping, while in the deflection optimization approach, the goal is to minimize the maximum deflection of the footbridge. The typical range of pedestrian walking frequencies falls between 1.6–2.4 Hz, see Ref. [45]. Hence, it is essential to calculate the maximum deflection of the footbridge and the energy absorbed by the DVA across a wide range of low frequencies. Utilizing a frequency domain representation is vital due to the random nature of walking parameters, including pedestrian frequencies, see Ref. [38]. Figure 6 provides a comparison between DVAs optimized according to energy and deflection criteria and DVA values from Den Hartog in the frequency domain.

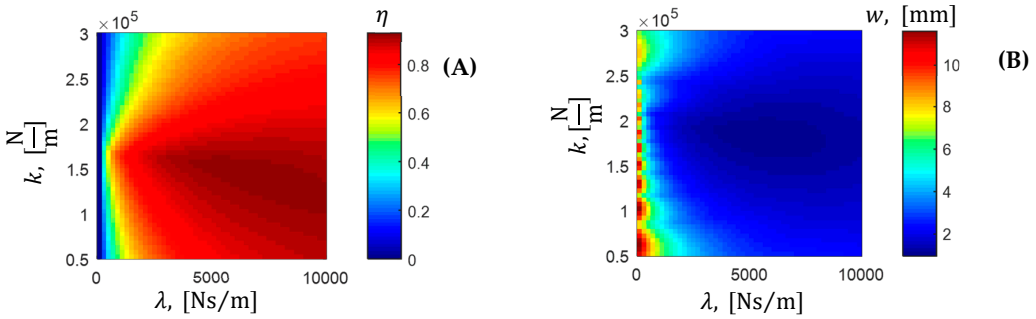

Figure 5. Parameters optimized for DVA. (**A**) Optimization method based on energy approach; (**B**) Optimization method based on deflection approach.

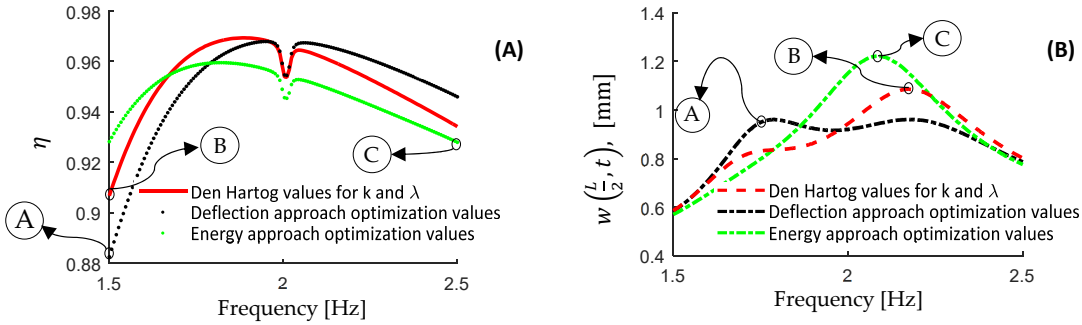

Figure 6. (**A**) The quantity of energy dissipated by linear DVAs; (**B**) Largest amount of displacement experienced by footbridges when subjected to linear DVAs in the frequency domain.

Peak points A, B, and C depicted in Figure 6 correspond to the optimized deflection approach DVA, linear DVA with Den Hartog values, and energy approach optimized DVA, respectively. These pivotal points signify the crucial frequencies that impact the determination of optimized parameters for both linear and nonlinear DVA methodologies. It should be emphasized that on the dissipated energy (η) graphs in Figure 6A, these points are associated with frequencies denoting the lowest dissipated energy, whereas on the deflection (w) graphs in Figure 6B, they indicate frequencies reflecting the highest deflections. Peak C in Figure 6A exhibits an energy dissipation of η = 92.822% in connection with energy approach optimization, surpassing peaks A and B associated with the deflection approach and Den Hartog method. The frequency dip observed at 2 Hz in Figure 6A is indicative of a resonance phenomenon. Within Figure 6B, Peak A illustrates the smallest deflection of 0.96 mm in the deflection approach method, which is lesser compared to peaks B and C. Additionally, in Figure 6B, the goal is to minimize the maximum deflection of the footbridge using different optimization methods across all frequencies related to a walking pedestrian.

4.1.2. The Optimal Configuration for Nonlinear DVAs

This section will investigate various forms of nonlinear DVAs based on the approaches outlined earlier. It is advisable to employ nonlinear DVAs when the excitation frequency varies. For instance, Starovetsky investigated a system with a nonlinear energy sink that exhibited quadratic damping characteristics [46]. In a separate study, Minaei and Ghorbani [47] introduced a novel variable stiffness mechanism that can be further developed as a practical nonlinear tool in engineering.

To investigate the effect of nonlinearity, the mathematical details of a DVA with quadratic stiffness and linear damping are checked with the parameters of elastic and damping forces defined as $\alpha = 1$, $\beta = 1$, $\gamma = 1$, and $\delta = 0$ (see Equations (11) and (12)). To optimize the nonlinear DVA parameters, the energy approach is utilized, yielding optimal

values of $\lambda = 9900\ \frac{\text{Ns}}{\text{m}}$ and $k = 2.4 \times 10^8\ \frac{\text{N}}{\text{m}^2}$ when $m = 2$ and $n = 0$ in Equation (13). Additionally, using the deflection approach, the following values are obtained: $\lambda = 4750\ \frac{\text{Ns}}{\text{m}}$, and $k = 1.55 \times 10^8\ \frac{\text{N}}{\text{m}^2}$. The maximum beam deflection and energy absorbed by the DVA are illustrated in Figure 7. Peak A in Figure 7B indicates a minimum deflection of 0.97 mm, which is lower than peaks B and C, suggesting that the DVA with quadratic stiffness and linear damping outperforms the linear DVA. As shown in Figure 7B, the optimized nonlinear DVA (dashed black line) consistently exhibits enhanced performance across the frequency range of 1.5 Hz to 2.5 Hz compared to the linear DVA using Den Hartog values. In Figure 7A, peak B (Den Hartog values) reflects an efficiency η = 90.68%, exceeding that of peaks C and A, which correspond to the energy and deflection approaches. The anti-peaks at 2 Hz are associated with a resonance phenomenon, indicating that, from an energy approach standpoint, this specific nonlinear DVA is less efficient than the linear DVA.

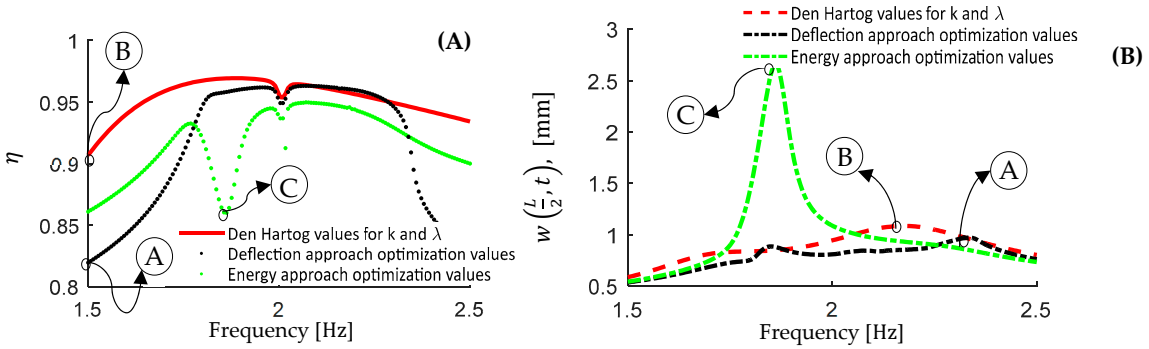

Figure 7. A footbridge connected to a Dynamic Vibration Absorber characterized by quadratic stiffness and linear damping in the frequency domain; (**A**) The quantity of energy dissipated by DVA (**B**) Maximum deflection of footbridge.

Now, the performance of a nonlinear DVA with quadratic stiffness and quadratic damping characteristics is investigated, see Figure 8. The maximum beam deflection and absorbed energy are presented in Figure 8. Notably, Figure 8A reveals a minor anti-peak at 1.88 Hz using the energy-optimized DVA, while a corresponding peak is evident in Figure 8B at point C. The integer powers for the elastic and damping forces in Equations (11) and (12) are set to $\alpha = 1$, $\beta = 1$, $\gamma = 1$, and $\delta = 1$, while in Equation (13), the values are $m = 2$ and $n = 1$. The peak A in Figure 8B indicates a minimum deflection of 0.97 mm, lower than the peaks B and C, suggesting better performance of the nonlinear DVA compared to the linear version. Optimal values obtained from the deflection approach optimization are $\lambda = 230\ \frac{\text{kNs}^2}{\text{m}^2}$ and $k = 150 \times 10^6\ \frac{\text{N}}{\text{m}^2}$, while those from the energy approach are $\lambda = 1350\ \frac{\text{kNs}^2}{\text{m}^2}$ and $k = 265 \times 10^6\ \frac{\text{N}}{\text{m}^2}$. As shown in Figure 8B, the nonlinear DVA consistently outperforms the linear model across most frequencies except within the ranges of 1.78 Hz to 1.83 Hz and 2.3 Hz to 2.4 Hz. Figure 8A indicates efficiency values of η = 90.68% for both Den Hartog and energy optimization methods, which exceed peak A from the deflection approach. The anti-peaks at 2 Hz result from resonance, indicating that this nonlinear DVA does not perform more efficiently than the linear one from an energy perspective.

Furthermore, Table 3 presents a detailed comparison of linear and nonlinear DVAs, demonstrating that the optimal parameters for minimizing deflection and maximizing energy absorption differ. This underscores the importance of defining the goals of the DVA before selecting its parameters. When the frequency of the applied excitation is variable, utilizing nonlinear DVAs is recommended [2]. Furthermore, although higher-order stiffness and damping nonlinearities (beyond cubic nonlinearity) were analyzed in this study, no significant improvements were identified, leading to their exclusion

for the sake of brevity. In addition to the aforementioned nonlinearity, various types of nonlinearities, including piecewise, polynomial, monomial, magnetorheological, and others, can be used as nonlinear elements for vibration reduction in bridges. For more information, please refer to Refs. [48–50].

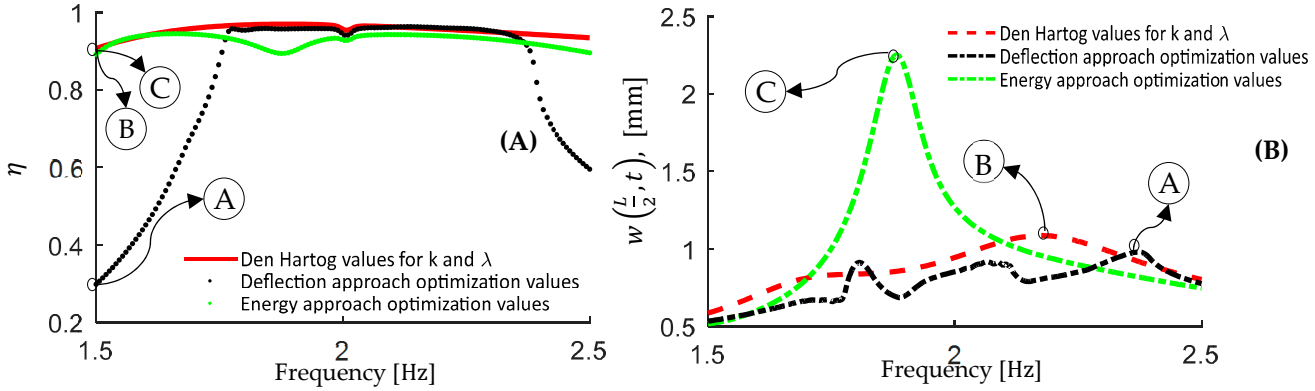

Figure 8. A footbridge equipped with a Dynamic Vibration Absorber exhibiting quadratic stiffness and quadratic damping characteristics in the frequency domain; (**A**) The energy dissipated by DVA, (**B**) Maximum deflection.

Table 3. Comparison between various optimization results under a walking pedestrian-induced excitation.

Footbridge and Type of DVA	Optimization Approach	Maximum Deflection [mm]	Minimum Value of Dissipated Energy [%]	Optimized k	Optimized λ	The Integers of Equations (11)–(13)
Bare footbridge	—	11.41	—	—	—	—
Linear DVA	Den Hartog values	1.1	90	164×10^3 $\frac{N}{m}$	5293 $\frac{Ns}{m}$	—
Linear DVA	Energy	1.2	92.82	145×10^3 $\frac{N}{m}$	6400 $\frac{Ns}{m}$	$m = 2$ and $n = 0$
Linear DVA	Deflection	0.96	88	180×10^3 $\frac{N}{m}$	6000 $\frac{Ns}{m}$	$\alpha = 1$, $\beta = 0$, $\gamma = 1$, and $\delta = 0$
Quadratic damping and linear stiffness	Energy	1.6	92.77	146×10^3 $\frac{N}{m}$	1.0×10^6 $\frac{Ns^2}{m^2}$	$m = 2$ and $n = 1$
Quadratic damping and linear stiffness	Deflection	0.96	66	183×10^3 $\frac{N}{m}$	0.42×10^6 $\frac{Ns^2}{m^2}$	$\alpha = 1$, $\beta = 0$, $\gamma = 1$, and $\delta = 1$
Quadratic stiffness and linear damping	Energy	2.6	86	240×10^6 $\frac{N}{m^2}$	9900 $\frac{Ns}{m}$	$m = 2$ and $n = 0$
Quadratic stiffness and linear damping	Deflection	0.97	82	155×10^6 $\frac{N}{m^2}$	4750 $\frac{Ns}{m}$	$\alpha = 1$, $\beta = 1$, $\gamma = 1$, and $\delta = 0$
Quadratic stiffness and damping	Energy	2.2	89	265×10^6 $\frac{N}{m^2}$	1.35×10^6 $\frac{Ns^2}{m^2}$	$m = 2$ and $n = 1$
Quadratic stiffness and damping	Deflection	0.97	30	150×10^6 $\frac{N}{m^2}$	0.23×10^6 $\frac{Ns^2}{m^2}$	$\alpha = 1$, $\beta = 1$, $\gamma = 1$, and $\delta = 1$
Cubic damping and linear stiffness	Energy	1.8	92	148×10^3 $\frac{N}{m}$	95×10^6 $\frac{Ns^3}{m^3}$	$m = 4$ and $n = 0$
Cubic damping and linear stiffness	Deflection	0.96	27	185×10^3 $\frac{N}{m}$	27.5×10^6 $\frac{Ns^3}{m^3}$	$\alpha = 1$, $\beta = 0$, $\gamma = 3$, and $\delta = 0$
Cubic stiffness and Linear damping	Energy	3.5	79	257×10^9 $\frac{N}{m^3}$	11700 $\frac{Ns}{m}$	$m = 2$ and $n = 0$
Cubic stiffness and Linear damping	Deflection	1.1	81	129×10^9 $\frac{N}{m^3}$	7750 $\frac{Ns}{m}$	$\alpha = 3$, $\beta = 0$, $\gamma = 1$, and $\delta = 0$
Cubic damping and Cubic stiffness	Energy	4.7	71	770×10^9 $\frac{N}{m^3}$	1.2×10^9 $\frac{Ns^3}{m^3}$	$m = 4$ and $n = 0$
Cubic damping and Cubic stiffness	Deflection	1.1	4	137×10^9 $\frac{N}{m^3}$	32×10^6 $\frac{Ns^3}{m^3}$	$\alpha = 3$, $\beta = 0$, $\gamma = 3$, and $\delta = 0$

4.2. The Impact of the Force Frequencies on the Optimization of the DVA Parameters

Equation (15) includes η_{1W}, η_{2W}, η_{3W}, and η_{4W} which are the initial four DLFs utilized in simulating a pedestrian walking behavior. Furthermore, DLFs for the first four harmonics are introduced to simulate a pedestrian engaged in running and jumping activities. The dataset derived from a previous study, [44], is subjected to cubic polynomial regression for analysis, and the findings are depicted in Figure 9. η_R and η_J are the DLFs for a pedestrian running and jumping. When the initial four DLFs for running and jumping are modeled using cubic polynomial regression, the Equations (18) and (19) are obtained for running and jumping pedestrians, respectively, as depicted by the solid lines in Figure 9.

$$\begin{aligned} \eta_{1R} &= -4.66 + 5.562\, f_p - 1.69(f_p)^2 + 0.1692(f_p)^3 \\ \eta_{2R} &= 4.791 - 2.688\, f_p + 0.5\,(f_p)^2 - 0.0295(f_p)^3 \\ \eta_{3R} &= 0.148 - 0.027 f_p + 0.0032\,(f_p)^2 - 0.000006(f_p)^3 \\ \eta_{4R} &= -2.790 + 1.326 f_p - 0.1223\,(f_p)^2 + 0.0047(f_p)^3 \end{aligned} \tag{18}$$

$$\begin{aligned} \eta_{1J} &= -0.776 + 2.533\, f_p - 0.8047(f_p)^2 + 0.077(f_p)^3 \\ \eta_{1J} &= -0.8647 + 0.7567\, f_p - 0.0879(f_p)^2 + 0.00132(f_p)^3 \\ \eta_{1J} &= 1.2552 - 0.6367\, f_p + 0.1194(f_p)^2 - 0.0068(f_p)^3 \\ \eta_{4J} &= 0.398 - 0.052 f_p - 0.0044\,(f_p)^2 + 0.0006(f_p)^3 \end{aligned} \tag{19}$$

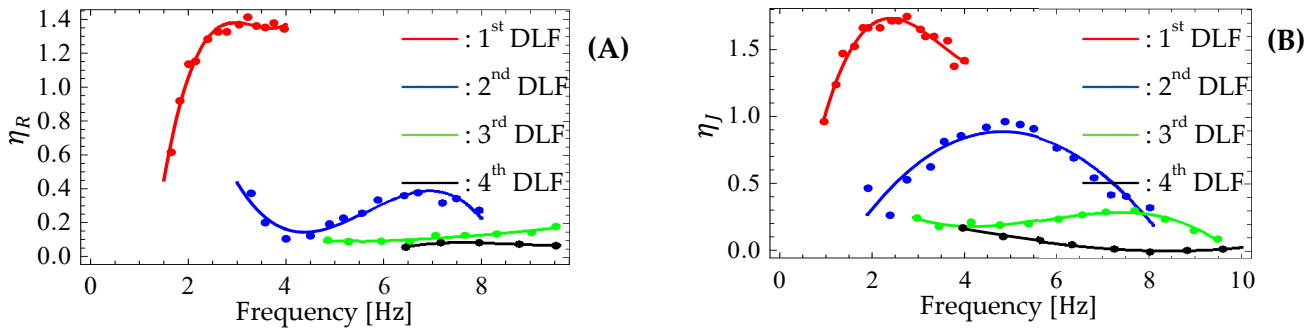

Figure 9. The initial four DLFs for (**A**) running pedestrian, and (**B**) jumping pedestrian.

In this study, the efficiency of a linear DVA optimized using the numerical deflection method is evaluated against analytical optimization techniques such as Den Hartog [51], Tigli [52], and Asami's H_∞ [53], as shown in Table 4. The primary goal of the H_∞ optimization criterion is to reduce the highest amplification factor based on [53]. The main goal of H_2 optimization is to reduce the squared area under the response curve of the main system. The results indicate that the maximum deflection of the footbridge during pedestrian activities is reduced when employing the numerical optimization approach used in this study, compared to the results from analytical approaches for the attached DVA. Table 4 demonstrates that the mechanical properties of the DVA vary under different types of excitations. Consequently, by utilizing a semi-active DVA that adjusts to surrounding conditions and excitation levels, significant reductions in bridge vibrations can be achieved. Notably, the optimization methods used in previous studies by Asami [53] (H_2 *and* H_∞), Tigli [52], and Den Hartog [51] focused on linear DVAs. Therefore, only the linear format of the DVA for the numerical optimization approach, is considered in Table 4.

Table 4. Comparison of different optimization results under different types of pedestrian excitations.

Case	Attached DVA	Optimization Approach	Type of Excitation	Maximum Deflection [mm]	Deflection Reduction vs. a Bare Footbridge %	Deflection Reduction Concerning Tigli's %	Deflection Reduction Concerning Den Hartog's %	Optimized Stiffness $k[\frac{kN}{m}]$	Optimized Damping $\lambda[\frac{kNs}{m}]$
1	×	–	Walking	10.30	–	–	–	–	–
2	✓	Numerical *	Walking	0.96	91	9	11	180	5.60
3	✓	Tigli	Walking	1.05	90	–	–	172	4.80
4	✓	Asami H_2	Walking	1.07	90	–	–	172	4.47
5	✓	Asami H_∞	Walking	1.09	90	–	–	163	5.30
6	✓	Den Hartog	Walking	1.08	90	–	–	164	5.29
7	×	–	Running	27.87	–	–	–	–	–
8	✓	Numerical *	Running	1.39	95	34	38	240	3.80
9	✓	Tigli	Running	2.11	92	–	–	172	4.80
10	✓	Asami H_2	Running	2.16	92	–	–	172	4.47
11	✓	Asami H_∞	Running	2.25	92	–	–	163	5.30
12	✓	Den Hartog	Running	2.24	92	–	–	164	5.29
13	×	–	Jumping	43.99	–	–	–	–	–
14	✓	Numerical *	Jumping	1.86	96	37	42	235	3.40
15	✓	Tigli	Jumping	2.95	93	–	–	172	4.80
16	✓	Asami H_2	Jumping	3.00	93	–	–	172	4.47
17	✓	Asami H_∞	Jumping	3.20	93	–	–	163	5.30
18	✓	Den Hartog	Jumping	3.18	93	–	–	164	5.29

Numerical *: considering the maximum deflection optimization approach by using Equations (1)–(12) in this study.

4.3. Review of Some Nonlinear DVAs

The parameters k and λ depend on the bridge's fundamental frequency, ω_1. Canter et al. [54] demonstrated that the natural frequencies of vehicle-bridge systems change with vehicle position, primarily due to a mass effect. This also applies to lightweight footbridges with pedestrians. Environmental factors affect structural stiffness and bridge frequency; Abdel-Wahab and Guido [55] observed that natural frequencies tend to increase as temperature decreases. Consequently, a passive vibration absorber may detune over time, therefore a variable damping and stiffness should be retuned automatically [56]. Additionally, Van Nimmen et al. [15] noted that, predicting a bridge's dynamic behavior is difficult due to uncertainties in parameters like stiffness of the supports of the bridge. They demonstrated that a deviation of 10% in the bridge's natural frequency can be expected compared to the predictions made by the finite element model. Temperature changes and long-term mechanical property variations also affect footbridge dynamics, as fluctuations can shift the modulus of elasticity for structural steel from 195 GPa to 205 GPa [57,58].

The aforementioned uncertainties are the motivation for introducing a new adjustable dashpot designed for use in a DVA, it is equipped with an actuator and motor and can be classified as a semi-active DVA.

As the nonlinearity can arise due to various reasons, such as the arrangement of the elements, which may be linear when considered individually, the structure of the element, and so on. In this work we propose two types of nonlinearities: geometric cubic nonlinearity and quadratic nonlinear damping.

4.3.1. Geometry Nonlinearity of Cubic Type

The nonlinear vibration absorber designed for the bridge is depicted in Figure 10.

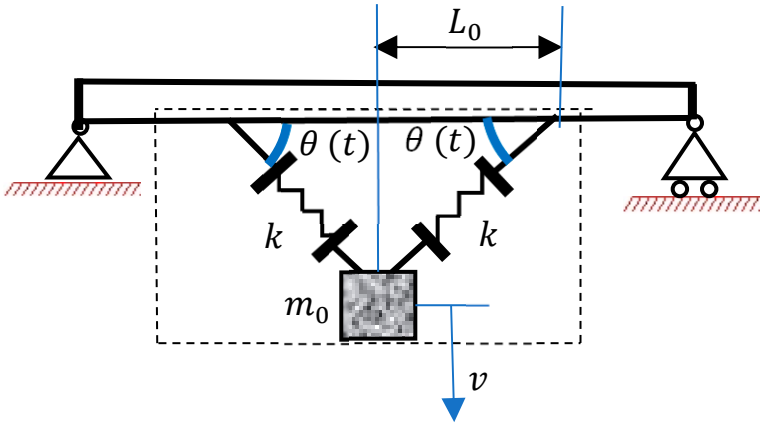

Figure 10. A DVA with geometric nonlinearity.

To determine the degree of nonlinearity in the specific nonlinear configuration of the system depicted in Figure 10, we take advantages from a previous study, Ref. [9], which results in cubic stiffness nonlinearity, while each connected spring is linear, the overall system connected exhibits cubic nonlinearity, the restoring force reads:

$$F = \frac{k}{{L_0}^2} v^3 + O\left(v^5\right) = Kv^3 + O\left(v^5\right) \tag{20}$$

Moreover, Minaei and Ghorbani [47] developed a variable stiffness element that can be incorporated into a DVA, transforming it into a semi-active device. Their work demonstrates the ability to change θ(t), as shown in Figure 10, which allows the stiffness element to be variable, thereby enabling the DVA to function as a semi-active nonlinear system with adjustable stiffness. Although cubic stiffness has been introduced here, there was no significant improvement for a footbridge subjected to pedestrian loads compared to an attached linear or quadratic stiffness. It was presented primarily to demonstrate how cubic nonlinearity can function in practice; for more information, refer to Table 3.

4.3.2. New Nonlinear Damper of Quadratic Type

This section describes a structurally nonlinear dashpot, accompanied by a schematic diagram that illustrates its main components. It can be classified as a semi-active quadratic variable damping dashpot. This type of dashpot can be used in a DVA as a quadratic damping element, enabling the adjustment of its parameters according to optimized values calculated to reduce bridge vibrations; see Table 3. As illustrated in Figure 11, the variable damping viscous damper (VDVD) comprises an outer cylinder, steel rods, an upper plate, and a truncated conical valve controlled by a handle threaded from inside. The main components of the dashpot are outlined here. The outer cylinder has a cylinder, five rods, and an upper plate. Each steel rod is connected to both the outer cylinder and the upper plate, forming a unit. A truncated conical valve slides along the rods to manage fluid flow. It has an internally threaded handle that passes through a hole in the upper plate. Inside the handle, an adjusting screw can rotate axially, and a motor on the inner cylinder turns this screw, moving the valve up or down. O-rings and bellows are used to prevent hydraulic oil leaks, ensuring the device is sealed.

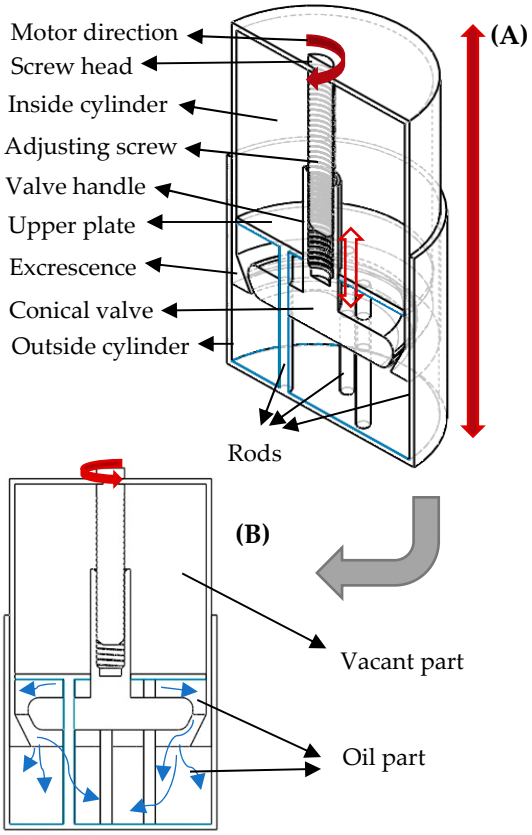

Figure 11. The VDVD is represented by a schematic diagram; (**A**) 3D model; (**B**) flowing of oil.

The benefits of the proposed nonlinear variable damping system in comparison to the orifice type include: (1) the system can handle a wide range of fluid flow rates and allows for variability in damping constants based on specific conditions; (2) unlike the orifice type, which can experience high-pressure drops and corrosion of thin plates leading to inaccuracies, the proposed system offers a more reliable and accurate solution for variable damping. The researchers studied how the damping force of the dashpot's two cylinders correlated with their relative velocity to identify the nonlinearity of the damper. The fluid moves through the channel as the cylinders are in motion, references [59,60] describe the equation for the fluid's volume flow rate Q through an orifice:

$$Q = \alpha(\Delta p)^{\frac{1}{2}} \tag{21}$$

$$Q = \rho\, V\, A \tag{22}$$

The equation in Figure 11B incorporates the experimental constant α specific to the fluid, the base area of both the conical valve and excrescence, along with the oil channel area. It relates to the pressure drop (Δp) between points 1 and 2. Equation (22) represents the fluid's volume flow rate through the channel, where the fluid's density is denoted as ρ, the relative velocity of the two cylinders is identified as V, and A is the surface area of the conical valve exposed to the fluid. By using Equations (21) and (22), it can be stated that:

$$V = \alpha(\Delta p)^{\frac{1}{2}}/\rho\, A \tag{23}$$

The external force exerted on the upper cylinder in Figure 11B results in a pressure variation between points 1 and 2. Hence, the total force acting on the conical valve and the excrescence can be calculated using the formula: $F = \Delta pA$; thus:

$$F = \frac{\rho^2 A^3}{\alpha^2} V^2 = \mathrm{c}\, V^2 \tag{24}$$

As presented in Equation (24), the damping force of the dashpot in Figure 11 is proportional to the square of the velocity, making it a quadratic nonlinear element. The damping constant, c, signifies this relationship. An actuator can control the motor's rotation, allowing the dashpot to provide various damping constants. This adaptability enables effective use of this nonlinear element in passive vibration absorbers, enhancing efficiency across a wide range of frequencies and highlighting a key advantage of nonlinear energy sinks.

5. Results and Discussion

This paper focuses on a case study involving bridge properties derived from Caprani et al. [61], who based their findings on Fujino et al.'s experimental research [62]. We consider a DVA attached to the bridge, emphasizing that its mechanical parameters should be tailored to the bridge type to ensure the model's adaptability across various structures. Furthermore, the response of the footbridge does not exhibit a linear relationship with the number of pedestrians. In the cases of marching troops, where nearly full synchronization occurs, the footbridge's response can be estimated by multiplying the response of a single pedestrian by $\sqrt{N}$. This suggests that in random crowds, pedestrians dampen each other's resonance effects, leading to reduced dynamic vibrations compared to scenarios with either a single pedestrian or a fully synchronized group.

Figure 12 represents a convergence analysis carried out using 1, 5 and 20 modal expansions, for the footbridge displacement field, with nonlinear DVA. For the sake of brevity, only two DVAs are selected: (1) quadratic damping and stiffness, and (2) quadratic stiffness and linear damping. In Figure 12A,B, the continuous red line indicates the footbridge response with five-mode expansion, while the black dotted line represents 20 modes. The results reveal no significant difference between the two expansions, indicating that modal interactions due to nonlinearity do not occur for excitation frequencies in the 1.5–2.5 Hz range. Frequencies above 3 Hz or below 1.25 Hz, are not investigated because they are outside typical walking excitation frequencies.

Furthermore, Sections 4.1–4.3 of this paper explore interesting findings about different types of nonlinear dampers using energy and deflection approach methods. It is worth noting that the specific results are presented in Table 3. Figure 7A presents the nonlinear DVA with quadratic stiffness and linear damping, showcasing a notable decrease in energy at point C, potentially due to superharmonic resonance. In Figure 7B, it is demonstrated that employing a DVA with quadratic stiffness and linear damping optimized through the deflection method leads to reduced deflection of the footbridge, outperforming a footbridge with a linearly attached DVA, across 92% of the frequency spectrum ranging from 1.5–2.5 Hz. The nonlinear DVA with quadratic damping and stiffness depicted by the dashed black line in Figure 8B performs better than the linear DVA with Den Hartog values in the entire frequency range analyzed, except for the intervals [1.78 Hz–1.83 Hz] and [2.3 Hz–2.4 Hz]. As a result, the deflection of the footbridge within the investigated frequency range of 1.5 to 2.5 Hz is lower in more than 86% of the frequency range, compared to the footbridge with the optimized linear DVA. The decrease in the absorbed energy at frequencies below 1.75 Hz is not due to resonance or superharmonic resonance, but rather to the optimization method and the associated mechanical values. To facilitate the

comparison, Figure 13 illustrates the maximum deflection of the footbridge equipped with an attached DVA, highlighting various types of nonlinearities. The effectiveness of the different types of nonlinear DVAs examined in this study on the maximum deflection of the footbridge is represented by distinct lines.

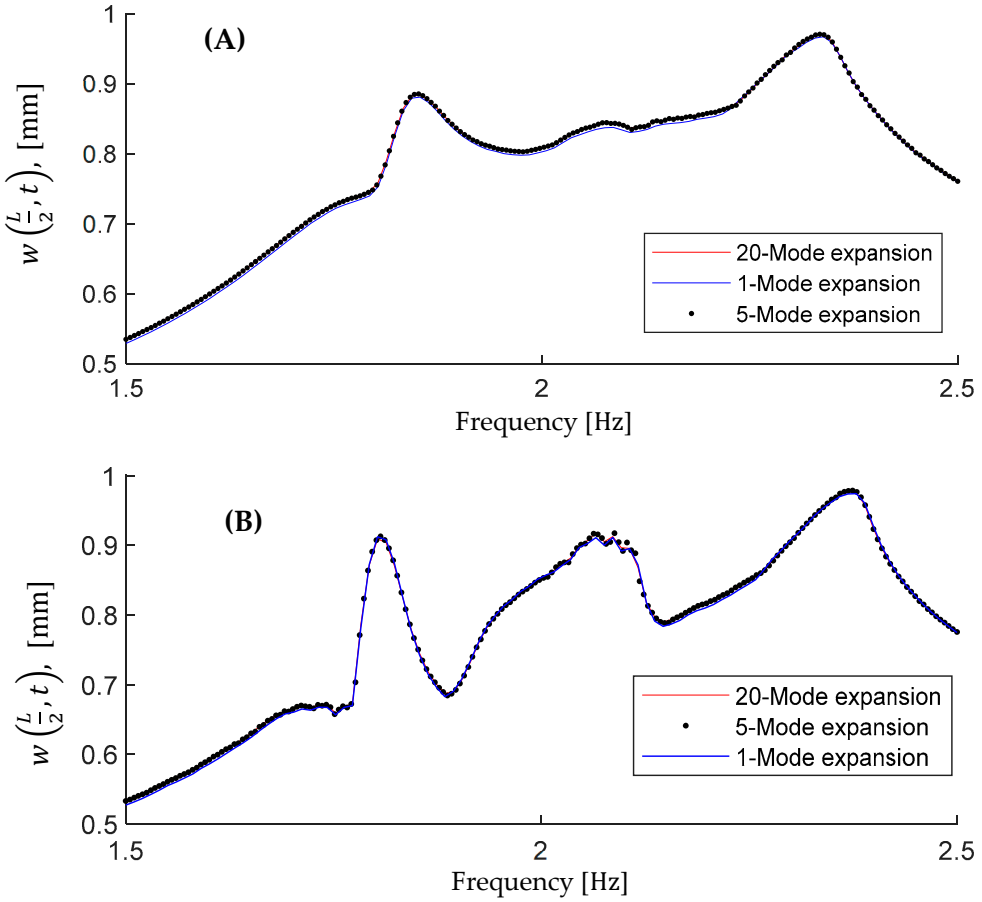

Figure 12. Evaluation of the nonlinearity of the DVAs on higher modes; (**A**): DVA with quadratic stiffness and linear damping elements; (**B**): DVA with both quadratic stiffness damping elements.

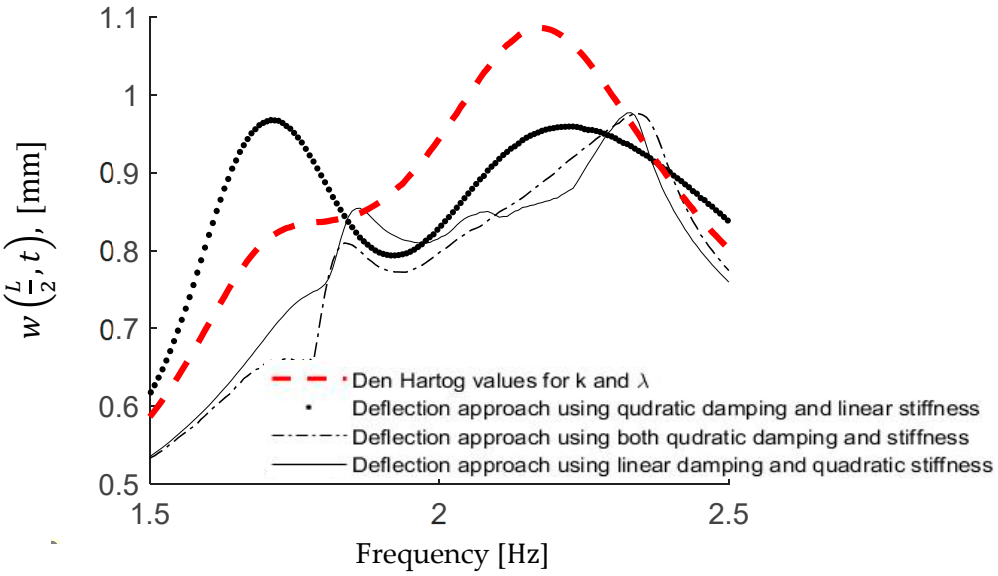

Figure 13. Comparison of a footbridge deflection equipped with various types of DVAs.

The results indicate that the optimal parameters for minimizing deflection and maximizing absorbed energy may be not similar. It is important to define the objective of using DVA and then select appropriate parameters; using a nonlinear DVA dampens the bridge's deflection over a wider range of frequencies versus a linear one. Note that, reference [2] suggests that increasing the power of nonlinear stiffness results in a more efficient reduction of beam deflection caused by vehicles. This study demonstrates that quadratic nonlinearities perform better when the beam is excited by pedestrians. Higher-order nonlinearities in stiffness and damping, are also studied, but no improvement was observed.

6. Conclusions

In this study, we explored the effectiveness of nonlinear semi-active dynamic vibration absorbers in mitigating vibrations of light bridges subjected to moving loads. The recent results show that those traditional passive absorbers are often weak in adjusting the damping and stiffness parameters of the DVA required for optimal performance in real-time conditions. Therefore, the introduction of nonlinear DVAs, particularly those with variable damping capabilities, presents a significant advancement in vibration control technology compared to traditional linear passive DVAs.

The main conclusion points of this research are listed as follow:

- The nonlinear DVAs, especially those with quadratic stiffness and linear damping, and DVA with both quadratic damping and stiffness elements, significantly reduce bridge deflections in a wider frequency range, compared to linear DVAs.
- The optimization of DVA parameters is pivotal for achieving the performant results in vibration reduction. In this study the two goal functions including, minimizing of the bridge displacement and maximizing of the amount of absorbed energy is considered.
- In the following, some of the challenges proposed for the future research, are listed:
- Exploring the design and implementation of active nonlinear dynamic vibration absorbers to enhance vibration control performance.
- Investigating the application of nonlinear quadratic stiffnesses to improve the effectiveness and responsiveness of vibration absorption systems.
- Investigating other types of nonlinear vibration absorbers attached to light footbridges, including piecewise linear stiffness or damping.
- Focus on developing semi-active or active control strategies that aim to minimize the damping time of vibrations and maximize the energy absorbed.
- The effects of various types of human activities specially the synchronized activities on the vibrations of the footbridges.

In conclusion, this study emphasizes the importance of selecting appropriate DVA parameters based on the desired objective, such as minimizing deflection or maximizing energy dissipation. Furthermore, Table 4 shows that by utilizing certain types of nonlinear DVAs, such as a numerically optimized DVA with both quadratic damping and stiffness, can reduce the vibrations of the bridge by approximately 40%.

Author Contributions: Conceptualization, F.P. and F.S.S.; methodology, F.P. and F.S.S.; software, H.S. and M.M.; validation, H.S. and F.S.S.; investigation, H.S., F.S.S. and F.P.; writing—original draft preparation, H.S., A.Z. and M.M.; writing—review and editing, H.S., F.S.S., A.Z. and F.P.; visualization, H.S. and M.M.; supervision, A.Z. and F.P.; project administration, A.Z. All authors have read and agreed to the published version of the manuscript.

Funding: This research received no external funding.

Data Availability Statement: The data that support the findings of this study are available from the corresponding author, [A.Z.], upon reasonable request.

Conflicts of Interest: The authors declare no conflict of interest.

Nomenclature

The following symbols are used in this paper:

W	weight of the pedestrian, [N]
m_p	pedestrian body mass, [kg]
g	gravity acceleration, [N/kg]
f_p	pedestrian pacing rate (pedestrian frequency), [Hz]
v_p	pedestrian velocity, [m/s]
l_p	step length of the pedestrian, [m]
η_k	coefficient of Fourier series named as "dynamic load factor (DLF)"
φ_k	harmonic phase angle
h	the number of harmonics
m_0	the mass of the dynamic vibration absorber (DVA), [kg]
$z(t)$	position of the DVA's mass
$w(x,t)$	vertical displacement of the beam
$u(t)$	the relative displacement of the DVA's mass and the footbridge mid-span
$G(t)$	passing pedestrian amplitude
$F(x,t)$	moving pedestrian-induced load
L	the length of the footbridge, [m]
E	modulus of elasticity of the footbridge, [GPa]
ξ_r	the damping ratio of the footbridge
$f(u)$	the force exerted by the DVA's spring, [N]
$g(u_{,t})$	viscous damping force, [N]
A	cross-section area, [m^2]
m	the footbridge mass per unit length, [m/kg]
I	moment of inertia, [m^4]
λ	damping coefficient, [kNs/m]
k	stiffness coefficient, [kN/m]
d	the location of the damper, [m]
ρ	the density of the footbridge material, [kg/m^3]
$q_r(t)$	modal coordinates
$\varphi_r(x)$	normalized eigenfunctions
N	the number of modes
ω_r	natural frequencies of the r^{th} mode of the footbridge, [rad/s]
m_e	footbridge equivalent mass, [kg]
μ	mass ratio

References

1. Samani, F.S.; Pellicano, F. Vibration reduction on beams subjected to moving loads using linear and nonlinear dynamic absorbers. *J. Sound Vib.* **2009**, *325*, 742. [CrossRef]
2. Samani, F.S.; Pellicano, F.; Masoumi, A. Performances of dynamic vibration absorbers for beams subjected to moving loads. *Nonlinear Dyn.* **2013**, *73*, 1065. [CrossRef]
3. Gatti, G. Fundamental insight on the performance of a nonlinear tuned mass damper. *Meccanica* **2018**, *53*, 111. [CrossRef]
4. Liu, P.; Zhu, H.-X.; Moaveni, B.; Yang, W.-G.; Huang, S.-Q. Vibration Monitoring of Two Long-Span Floors Equipped with Tuned Mass Dampers. *Int. J. Struct. Stab. Dyn.* **2019**, *19*, 1950101. Available online: https://worldscientific.com/doi/abs/10.1142/S0219455419501013 (accessed on 23 December 2024). [CrossRef]
5. Samani, F.S.; Pellicano, F. Vibration reduction of beams under successive traveling loads by means of linear and nonlinear dynamic absorbers. *J. Sound Vib.* **2012**, *331*, 2272. [CrossRef]
6. Saber, H.; Samani, F.S.; Pellicano, F. Vibration reduction of footbridges subjected to walking, running, and jumping pedestrian. *J. Vib. Control* **2023**, *29*, 3227. [CrossRef]

7. Chen, Z.; Chen, Z.; Li, G.; Zhang, W.; Zhang, X.; Huang, S.; Chen, Z. Dynamic Response Analysis and Vibration Reduction of Steel Truss Corridor Pedestrian Bridge Under Pedestrian Load. *Front. Mater.* **2022**, *9*, 839265. [CrossRef]
8. Bassoli, E.; Vincenzi, L. Parameter calibration of a social force model for the crowd-induced vibrations of footbridges. *Front. Built Environ.* **2021**, *7*, 656799. [CrossRef]
9. Saber, H.; Samani, F.S.; Pellicano, F. Nonlinear vibration absorbers applied on footbridges. *Meccanica* **2021**, *56*, 23. [CrossRef]
10. Caprani, C.C.; Ahmadi, E. Formulation of human–structure interaction system models for vertical vibration. *J. Sound Vib.* **2016**, *377*, 346. [CrossRef]
11. Ao, W.K.; Reynolds, P. (Eds.) Analytical and experimental study of eddy current damper for vibration suppression in a footbridge structure. In *Dynamics of Civil Structures*; Springer: Berlin/Heidelberg, Germany, 2017; Volume 2. [CrossRef]
12. Ao, W.K.; Reynolds, P. Analysis and numerical evaluation of H∞ and H2 optimal design schemes for an electromagnetic shunt damper. *J. Vib. Acoust.* **2020**, *142*, 021003. [CrossRef]
13. Pedersen, L.; Frier, C. Stochastic Load Models and Footbridge Response. *Dyn. Civ. Struct.* **2015**, *2*, 75. [CrossRef]
14. Lievens, K.; Lombaert, G.; De Roeck, G.; Van den Broeck, P. Robust design of a TMD for the vibration serviceability of a footbridge. *Eng. Struct.* **2016**, *123*, 408. [CrossRef]
15. Van Nimmen, K.; Lombaert, G.; De Roeck, G.; Van den Broeck, P. Vibration serviceability of footbridges: Evaluation of the current codes of practice. *Eng. Struct.* **2014**, *59*, 448. [CrossRef]
16. Ding, H.; Chen, L.-Q. Designs, analysis, and applications of nonlinear energy sinks. *Nonlinear Dyn.* **2020**, *100*, 3061. [CrossRef]
17. Gourdon, E.; Lamarque, C.-H.; Pernot, S. Contribution to efficiency of irreversible passive energy pumping with a strong nonlinear attachment. *Nonlinear Dyn.* **2007**, *50*, 793. [CrossRef]
18. Ferreira, F.; Moutinho, C.; Cunha, Á.; Caetano, E. Use of semi-active tuned mass dampers to control footbridges subjected to synchronous lateral excitation. *J. Sound Vib.* **2019**, *446*, 176. [CrossRef]
19. Maślanka, M. Optimised semi-active tuned mass damper with acceleration and relative motion feedbacks. *Mech. Syst. Signal Process.* **2019**, *130*, 707. [CrossRef]
20. Saber, H.; Samani, F.S.; Pellicano, F. A novel nonlinear variable damping device and its application for the systems with uncertain parameters. *Proc. Inst. Mech. Eng. Part K J. Multi-Body Dyn.* **2022**, *236*, 660. [CrossRef]
21. Chen, J.; Han, Z.; Xu, R. Effects of human-induced load models on tuned mass damper in reducing floor vibration. *Adv. Struct. Eng.* **2019**, *22*, 2449. [CrossRef]
22. Nguyen, K.; Soria, J.M.; Díaz, I.M.; Goicolea, J.M. Exploring the potential of the semi-active inertial absorber in control resonant effects for short-to-medium span high-speed railway bridges. *Struct. Infrastruct. Eng.* **2023**, 1–16. [CrossRef]
23. Kumar, J.; Bhushan, G. Modelling of a semi-active vibration absorber featuring variable stiffness and variable damping using magnetorheological materials. *Mater. Today Proc.* **2023**, in press. [CrossRef]
24. Barrera-Vargas, C.A.; Naranjo-Pérez, J.; Díaz, I.M.; García-Palacios, J.H. Design of a Semiactive TMD for Lightweight Pedestrian Structures Considering Human–Structure–Actuator Interaction. *Actuators* **2022**, *11*, 101. [CrossRef]
25. Wang, J.; Zhang, X.; Liu, Y.; Qin, Z.; Ma, L.; Hong, F.; Chu, F. Dynamic analysis of magnetorheological damper incorporating elastic ring in coupled multi-physical fields. *Mech. Syst. Signal Process.* **2024**, *208*, 111040. [CrossRef]
26. Javani, M.; Eslami, M.R.; Kiani, Y. Active control of thermally induced vibrations of temperature-dependent FGM circular plate with piezoelectric sensor/actuator layers. *Aerosp. Sci. Technol.* **2024**, *146*, 108997. [CrossRef]
27. Jiang, X.; McFarland, D.M.; Bergman, L.A.; Vakakis, A.F. Steady state passive nonlinear energy pumping in coupled oscillators: Theoretical and experimental results. *Nonlinear Dyn.* **2003**, *33*, 87. [CrossRef]
28. Yang, Y.; Wang, X. Investigation into the linear velocity response of cantilever beam embedded with impact damper. *J. Vib. Control* **2019**, *25*, 1365. [CrossRef]
29. Wang, J.; Wang, B.; Liu, Z.; Zhang, C.; Li, H. Experimental and numerical studies of a novel asymmetric nonlinear mass damper for seismic response mitigation. *Struct. Control Health Monit.* **2020**, *27*, e2513. [CrossRef]
30. Wang, L.; Zhou, Y.; Shi, W. Random crowd-induced vibration in footbridge and adaptive control using semi-active TMD including crowd-structure interaction. *Eng. Struct.* **2024**, *306*, 117839. [CrossRef]
31. Wu, J.-J. Study on the inertia effect of helical spring of the absorber on suppressing the dynamic responses of a beam subjected to a moving load. *J. Sound Vib.* **2006**, *297*, 981. [CrossRef]
32. Zienkiewicz, O.C. RLTaJZZ. In *The Finite Element Method: Its Basis and Fundamentals*; Elsevier: Amsterdam, The Netherlands, 2013.
33. Reddy, J.N. *An Introduction to the Finite Element Method*; McGraw-Hill: New York, NY, USA, 2005.
34. Khurshudyan, A.; Ohanyan, S. (Eds.) Vibrations of geometrically nonlinear beam subjected to two oppositely moving loads and supported by three equidistant visco-elastic dampers. *J. Phys. Conf. Ser.* **2018**, *991*, 012046. [CrossRef]
35. Szafrański, M. Vibration of the bridge under moving singular loads-theoretical formulation and numerical solution. *J. Appl. Math. Comput. Mech.* **2016**, *15*, 169. [CrossRef]
36. Vakakis, A.F.; Manevitch, L.; Gendelman, O.; Bergman, L. Dynamics of linear discrete systems connected to local, essentially non-linear attachments. *J. Sound Vib.* **2003**, *264*, 559. [CrossRef]

37. Sayyad, F.; Gadhave, N. Variable stiffness type magnetic vibration absorber to control the vibration of beam structure. *J. Vib. Control* **2014**, *20*, 1960. [CrossRef]
38. Pedersen, L.; Frier, C. Sensitivity of footbridge vibrations to stochastic walking parameters. *J. Sound Vib.* **2010**, *329*, 2683. [CrossRef]
39. Fujino, Y.; Siringoringo, D.M. A conceptual review of pedestrian-induced lateral vibration and crowd synchronization problem on footbridges. *J. Bridge Eng.* **2016**, *21*, C4015001. [CrossRef]
40. Racic, V.; Brownjohn, J.M.W. Stochastic model of near-periodic vertical loads due to humans walking. *Adv. Eng. Inform.* **2011**, *25*, 259. [CrossRef]
41. Young, P. Improved floor vibration prediction methodologies. In Proceedings of the Arup Vibration Seminar on Engineering for Structural Vibration—Current Developments in Research and Practice, London, UK, 1 October 2001.
42. Kim, S.-H.; Cho, K.-I.; Choi, M.-S.; Lim, J.-Y. Development of human body model for the dynamic analysis of footbridges under pedestrian induced excitation. *Steel Struct.* **2008**, *8*, 333.
43. Wu, Q.; Kitahara, Y.; Takahashi, K.; Chen, B. Dynamic characteristics of Megami cable-stayed bridge: A comparison of experimental and analytical results. *Int. J. Steel Struct.* **2008**, *8*, 1–9.
44. Rainer, J.; Pernica, G.; Allen, D.E. Dynamic loading and response of footbridges. *Can. J. Civ. Eng.* **1988**, *15*, 66. [CrossRef]
45. Živanović, S.; Pavic, A.; Reynolds, P. Vibration serviceability of footbridges under human-induced excitation: A literature review. *J. Sound Vib.* **2005**, *279*, 1–74. [CrossRef]
46. Starosvetsky, Y.; Gendelman, O. Vibration absorption in systems with a nonlinear energy sink: Nonlinear damping. *J. Sound Vib.* **2009**, *324*, 916. [CrossRef]
47. Minaei, A.; Ghorbani-Tanha, A. Optimal step-by-step tuning method for variable stiffness semiactive tuned mass dampers. *J. Eng. Mech.* **2019**, *145*, 04019037. [CrossRef]
48. Nayfeh, A.H.; Mook, D.T. *Nonlinear Oscillations*; John Wiley & Sons: Hoboken, NJ, USA, 2024.
49. Vakakis, A.F.; Gendelman, O.V.; Bergman, L.A.; McFarland, D.M.; Kerschen, G.; Lee, Y.S. *Nonlinear Targeted Energy Transfer in Mechanical and Structural Systems*; Springer Science & Business Media: Berlin/Heidelberg, Germany, 2008.
50. Ye, X.; Ni, Y.-Q.; Ao, W.K.; Yuan, L. Modeling of the hysteretic behavior of nonlinear particle damping by Fourier neural network with transfer learning. *Mech. Syst. Signal Process.* **2024**, *208*, 111006. [CrossRef]
51. Den Hartog, J.P. *Mechanical Vibrations*; Courier Corporation: Chelmsford, MA, USA, 1985.
52. Tigli, O.F. Optimum vibration absorber (tuned mass damper) design for linear damped systems subjected to random loads. *J. Sound Vib.* **2012**, *331*, 3035. [CrossRef]
53. Asami, T.; Nishihara, O. Closed-form exact solution to H∞ optimization of dynamic vibration absorbers (application to different transfer functions and damping systems). *J. Vib. Acoust.* **2003**, *125*, 398. [CrossRef]
54. Cantero, D.; McGetrick, P.; Kim, C.-W.; OBrien, E. Experimental monitoring of bridge frequency evolution during the passage of vehicles with different suspension properties. *Eng. Struct.* **2019**, *187*, 209. [CrossRef]
55. Wahab, M.A.; De Roeck, G. Effect of temperature on dynamic system parameters of a highway bridge. *Struct. Eng. Int.* **1997**, *7*, 266. [CrossRef]
56. Zhang, L.; Hong, L.; Dhupia, J.S.; Johnson, S.; Qaiser, Z.; Zhou, Z. (Eds.) A novel semi-active tuned mass damper with tunable stiffness. In Proceedings of the IEEE/ASME International Conference on Advanced Intelligent Mechatronics (AIM), Auckland, New Zealand, 9–12 July 2018; IEEE: Piscataway, NJ, USA, 2018. [CrossRef]
57. Ledbetter, H. Stainless-steel elastic constants at low temperatures. *J. Appl. Phys.* **1981**, *52*, 1587. [CrossRef]
58. Wagner, D.; Cavalieri, F.J.; Bathias, C.; Ranc, N. Ultrasonic fatigue tests at high temperature on an austenitic steel. *Propuls. Power Res.* **2012**, *1*, 29. [CrossRef]
59. Munson, B.R.; Young, D.F.; Okiishi, T.H.; Huebsch, W.W. *Fundamentals of Fluid Mechanics*; John Wiley & Sons, Inc.: Hoboken, NJ, USA, 2006.
60. Rao, S.S. *Mechanical Vibrations*; Pearson Education: Singapore, 2011.
61. Caprani, C.C.; Keogh, J.; Archbold, P.; Fanning, P. Enhancement factors for the vertical response of footbridges subjected to stochastic crowd loading. *Comput. Struct.* **2012**, *102*, 87. [CrossRef]
62. Fujino, Y.; Pacheco, B.M.; Nakamura, S.I.; Warnitchai, P. Synchronization of human walking observed during lateral vibration of a congested pedestrian bridge. *Earthq. Eng. Struct. Dyn.* **1993**, *22*, 741. [CrossRef]